



Synthesis and characterization of copper(II) dithiocarbamate complexes involving pyrrole and ferrocenyl moieties and their utility for sensing anions and preparation of copper sulfide and copper–iron sulfide nanoparticles

Govindasamy Gurumoorthy¹ | Subbiah Thirumaran¹ | Samuele Ciattini²

¹Department of Chemistry, Annamalai University, Annamalaiagar, -608 002, India

²Centro di Cristallografia Strutturale, Polo Scientifico di Sesto Fiorentino, Via della Lastruccia 3, 50019 Sesto Fiorentino, Florence, Italy

Correspondence

Subbiah Thirumaran, Department of Chemistry, Annamalai University, Annamalaiagar – 608 002, India. Email: sthirumaran@yahoo.com

Funding information

University Grants Commission (UGC), India, Grant/Award Number: F. No. 42-341/2013 (SR)

Bis(*N*-(pyrrol-2-ylmethyl)-*N*-butyldithiocarbamato-*S,S'*)copper(II) (**1**), bis(*N*-(pyrrol-2-ylmethyl)-*N*-(2-phenylethyl)dithiocarbamato-*S,S'*)copper(II) (**2**), bis(*N*-methylferrocenyl-*N*-(2-phenylethyl)dithiocarbamato-*S,S'*)copper(II) (**3**) and bis(*N*-furfuryl-*N*-methylferrocenyldithiocarbamato-*S,S'*)copper(II) (**4**) were prepared and characterized using elemental analysis and infrared and UV–visible spectroscopies. X-ray diffraction (XRD) studies on **3** show that each copper centre adopts the square planar geometry by the coordination of four sulfur atoms of the metalloligand *N*-methylferrocenyl-*N*-(2-phenylethyl)dithiocarbamate. The Cu–S distances are symmetrical and are in the range 2.293–2.305 Å. The supramolecular architecture in complex **3** is sustained in the solid state by C–H⋯π, C–H⋯S, Fe⋯Fe and H⋯H interactions. Density functional theory calculations were carried out for **3**. Anion (F[−], Cl[−], Br[−] and I[−]) binding studies with complex **1** were performed using cyclic voltammetry. Copper sulfide, copper–iron sulfide-**1** and copper–iron sulfide-**2** nanoparticles were prepared from complexes **2**, **3** and **4**, respectively, and they were characterized using powder XRD, transmission electron microscopy (TEM) and energy-dispersive X-ray, UV–visible, photoluminescence and infrared spectroscopies. TEM images of copper–iron sulfide-**1** and copper–iron sulfide-**2** reveal that the particles are spherical and oval shaped, respectively. Photocatalytic activities of as-prepared nanoparticles were studied by decolourization of methylene blue and rhodamine-B under UV light. It was found that copper–iron sulfide degrades methylene blue and rhodamine-B much better than does copper sulfide.

KEYWORDS

anion sensing, copper sulfide, copper(II) dithiocarbamates, copper–iron sulfide, photodegradation

1 | INTRODUCTION

Dithiocarbamate ligands have found ample use in coordination chemistry.^[1,2] Their wide range of applications such as in industry, agriculture and medicine have generated a large collection of crystallographic data for their metal complexes.^[3–6] Dithiocarbamates are versatile ligands capable of stabilizing transition metals in both high and low oxidation states,^[7] and complexes of Cu(I), Cu(II) and Cu(III) are all known, being interconvertible via reversible one-electron redox process.^[8] Electrochemical studies of these complexes reveal that they can sense various anions and cations.^[9] Modifications in the R groups attached to nitrogen atom of the dithiocarbamate fragment can have an effect on both the structure and chemical properties, mainly due to a change in the acid–base nature of the dithiocarbamate fragment.^[10] A number of copper dithiocarbamate complexes have been shown to be efficient catalysts for the atom-transfer radical polymerization and reverse atom-transfer radical polymerization of methyl methacrylate.^[11,12] Recently, copper(II) complexes containing ferrocenyl-based dithiocarbamates have been exploited as sensitizers in dye-sensitized TiO₂ solar cells for converting sunlight into electrical energy.^[13] In recent years, copper dithiocarbamate complexes have been used as single-source precursors for the preparation of copper sulfides^[14–18] and in ferroelectric materials,^[19] electrochemical sensors,^[20] photoconductivity,^[21] a wealth of metal-centred electrochemistry^[2,22] and interesting photochemistry.^[7,23] Metal sulfides can also serve as important semiconductor photocatalysts which offer the potential for complete elimination of toxic chemicals.

Herein we report the synthesis, characterization and anion-sensing properties of copper(II) dithiocarbamate complexes containing pyrrole and ferrocene moieties. In addition, the synthesis, characterization and photocatalytic activities of copper sulfide and copper–iron sulfide nanoparticles, which were synthesized from the as-prepared complexes, are also presented.

2 | EXPERIMENTAL

2.1 | Materials and Techniques

Reagent-grade chemicals were purchased from commercial sources and used as such. Infrared (IR) spectra were recorded with a Thermo Nicolet Avatar 330 FT-IR spectrophotometer (range: 400–4000 cm⁻¹) as KBr pellets. A Shimadzu UV-1650 PC double-beam UV–visible spectrophotometer was used for recording the electronic spectra. The spectra of complexes were recorded in CHCl₃ and the pure solvent was used as the reference. Powder X-ray

diffraction (XRD) was performed using an EQUINOX 1000. Transmission electron microscopy (TEM) images were recorded using a TECNAI T2 G2 (FEI). Energy-dispersive X-ray spectroscopy (EDS) was performed with a SUPRA 55VP CARL. Photoluminescence spectra were recorded using a PerkinElmer 1555 fluorescence spectrophotometer at room temperature.

2.2 | X-ray Crystallography

Diffraction data were recorded with a SuperNova, Dual, Cu at zero, Pilatus 200/300 K diffractometer using graphite-monochromated Cu K α radiation ($\lambda = 1.54184 \text{ \AA}$) at ambient temperature. The structure was solved and refined by direct method using SHELXL-2014/7.^[24] All non-hydrogen atoms were refined anisotropically and the hydrogen atoms were refined isotropically. Details of the crystal data and structure refinement parameters for **3** are summarized in Table 1. Selected bond lengths and angles for **3** are given in Table 2.

2.3 | Theoretical Calculations

The highest occupied molecular orbital (HOMO)–lowest unoccupied molecular orbital (LUMO) energy was calculated with the Gaussian 03 software package using gradient-corrected density functional theory (DFT) with the B3LYP method.^[25] The LANL2DZ basis set was used by including effective core potential functions.

2.4 | Cyclic Voltammetry

Cyclic voltammetry was performed using a conventional three-electrode system. A glassy carbon electrode was used as a working electrode. The counter electrode was a platinum wire and the reference electrode was Ag/AgCl. HPLC-grade acetonitrile was used as the solvent and tetrabutylammonium fluoroborate (0.01 M) as the supporting electrolyte. The scan rate was 100 mV s⁻¹. Complex **3** was investigated at 25 °C in an oxygen-free atmosphere, provided by bubbling purified nitrogen through the solution. The concentration of the compounds was 1×10^{-4} M in electrochemical solutions of (*n*-Bu₄N)I, (*n*-Bu₄N)Br, (*n*-Bu₄N)Cl and (*n*-Bu₄N)F (5×10^{-4} M) in acetonitrile. Cyclic voltammograms were recorded with a CHI604C Electrochemical Analyser.

2.5 | Photocatalytic Experiments

The photocatalytic activity of copper sulfide and copper–iron sulfide was evaluated by degradation of aqueous solutions of methylene blue and rhodamine-B. All the solutions were prepared using double-distilled water.

TABLE 1 Crystal data, data collection and refinement parameters for complex **3**

Empirical formula	$C_{40}H_{40}CuFe_2N_2S_4$	
Formula weight	852.22	
Crystal dimensions (mm ³)	0.30 × 0.20 × x 0.20	
Crystal system	Monoclinic	
Space group	P2 _{1/n}	
<i>a</i> (Å)	12.5771(3)	
<i>b</i> (Å)	23.3141(7)	
<i>c</i> (Å)	12.9515(3)	
α (°)	90	
β (°)	108.725(2)	
γ (°)	90	
<i>V</i> (Å ³)	3596.68(17)	
<i>Z</i>	4	
<i>D_c</i> (g cm ⁻³)	1.574	
μ (cm ⁻¹)	9.489	
<i>F</i> (000)	1756	
λ (Å)	Cu K α (1.54184)	
θ range (°)	3.792 to 75.061	
Index ranges	-15 ≤ <i>h</i> ≤ 15, -28 ≤ <i>k</i> ≤ 26, -16 ≤ <i>l</i> ≤ 16	
Reflections collected	70 965	
Observed reflections [<i>I</i> > 2 σ (<i>I</i>)]	6452	
Weighting scheme	Calc. $W = 1/[\sigma^2(F_o^2) + (0.0420P)^2 + 1.9063P]$, where $p = (F_o^2 + 2F_c^2)/3$	
$R[F^2 > 2\sigma(F^2)]$, $wR(F^2)$	0.0319, 0.0845	
Number of parameters refined	442	
GOF	1.09	

TABLE 2 Selected bond lengths (Å) and bond angles (°) of **3**

Bond length	XRD	DFT/LanL2DZ	Bond angle	XRD	DFT/LanL2DZ
Cu–S4	2.2937(6)	2.431	S4–Cu–S2	102.03(2)	103.49
Cu–S2	2.2986(6)	2.492	S4–Cu–S3	77.75(2)	76.50
Cu–S3	2.3023(6)	2.430	S2–Cu–S3	170.06(3)	179.93
Cu–S1	2.3052(6)	2.432	S4–Cu–S1	176.90(3)	179.93
S1–C1	1.727(2)	1.790	S2–Cu–S1	77.56(2)	76.49
S3–C21	1.723(2)	1.792	S3–Cu–S1	103.19(2)	103.50
S2–C1	1.719(2)	1.792	N1–C1–S2	123.57(16)	123.18
S4–C21	1.729(2)	1.705	N1–C1–S1	122.86(16)	122.53
N1–C1	1.315(3)	1.344	N2–C21–S3	124.49 (16)	123.21
N2–C21	1.316(3)	1.344	N2–C21–S4	122.14 (16)	122.49

For a typical photocatalytic experiment, 0.1 g of catalyst was added to 50 ml of an aqueous solution of rhodamine-B at a concentration of 1.0×10^{-4} M. The solution was maintained in the dark for 30 min to reach dye

solution adsorption–desorption equilibrium. The solution with the suspended nano-photocatalyst was irradiated by UV light from a mercury vapour lamp. At given time intervals, 3 ml aliquots were withdrawn and centrifuged

to remove catalyst. The concentration of dye solution was determined using a UV-visible spectrophotometer.

3 | PREPARATION OF COMPLEXES

3.1 | Preparation of Amines

N-(Pyrrol-2-ylmethyl)-*N*-butylamine, *N*-(pyrrol-2-ylmethyl)-*N*-(2-phenylethyl)amine, *N*-methylferrocenyl-*N*-(2-phenylethyl)amine and *N*-furfuryl-*N*-methylferrocenylamine were prepared by general methods reported earlier.^[26]

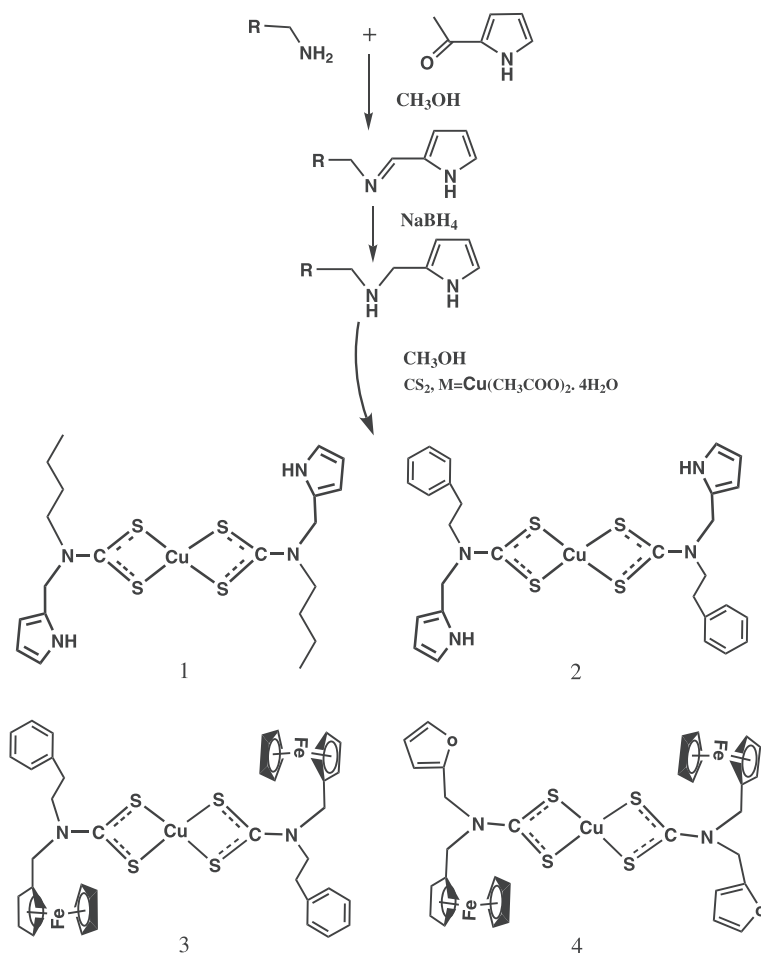
3.2 | Preparation of Bis(*N*-(pyrrol-2-ylmethyl)-*N*-butyldithiocarbamato-*S,S'*)copper(II) (1)

N-(Pyrrol-2-ylmethyl)-*N*-butylamine (4.0 mmol, 0.9 ml) in ethanol was mixed with carbon disulfide (4.0 mmol, 0.3 ml) under ice-cold conditions (5°C). The solution was stirred for 30 min. This produced the *N*-(pyrrol-2-ylmethyl)-*N*-butyldithiocarbamic acid solution. An aqueous solution of $\text{Cu}(\text{CH}_3\text{COO})_2 \cdot \text{H}_2\text{O}$ (2.0 mmol, 0.3993 g)

was added to the dithiocarbamic acid solution resulting in the formation of a brown precipitate. The precipitate obtained was filtered, washed several times with cold water and then air-dried (Scheme 1). Yield: 78%, m.p. 149–151°C. IR (KBr, ν , cm^{-1}): 3381 ($\nu_{\text{N-H}}$), 1494 ($\nu_{\text{C-N}}$), 1029 ($\nu_{\text{C-S}}$). UV-visible (CHCl_3 , λ , nm): 634, 439, 275, 244; Anal. Calcd for $\text{C}_{20}\text{H}_{23}\text{CuN}_4\text{S}_4$ (%): C, 46.35; H, 5.83; N, 10.81; found (%): C, 46.18; H, 5.77; N, 10.75.

3.3 | Preparation of Bis(*N*-(pyrrol-2-ylmethyl)-*N*-(2-phenylethyl)dithiocarbamato-*S,S'*)copper(II) (2)

A method similar to that described for the synthesis of 1 was adopted; however, *N*-(pyrrol-2-ylmethyl)-*N*-(2-phenylethyl)amine was used instead of *N*-(pyrrol-2-ylmethyl)-*N*-butylamine (Scheme 1). Colour: brown; yield: 80%; m.p. 153–155°C. IR (KBr, ν , cm^{-1}): 3388 ($\nu_{\text{N-H}}$), 1490 ($\nu_{\text{C-N}}$), 1025 ($\nu_{\text{C-S}}$). UV-visible (CHCl_3 , λ , nm): 639, 438, 275, 237; Anal. Calcd for $\text{C}_{28}\text{H}_{30}\text{CuN}_4\text{S}_4$ (%): C, 54.74; H, 4.92; N, 9.12; found (%): C, 54.60; H, 4.89; N, 9.06.



SCHEME 1 Preparation of complexes 1, 2, 3 and 4

3.4 | Preparation of Bis(*N*-methylferrocenyl-*N*-(2-phenylethyl)dithiocarbamato-*S,S'*)copper(II) (3)

A method similar to that described for the synthesis of **1** was adopted; however, *N*-methylferrocenyl-*N*-(2-phenylethyl)amine used instead of *N*-(pyrrol-2-ylmethyl)-*N*-butylamine (Scheme 1). Colour: brown; yield: 76%; m. p. 165–167°C. IR (KBr, ν , cm^{-1}): 1490 ($\nu_{\text{C-N}}$), 1025 ($\nu_{\text{C-S}}$). UV-visible (CHCl_3 , λ , nm): 630, 428, 271, 237: Anal. Calcd for $\text{C}_{40}\text{H}_{40}\text{CuFe}_2\text{N}_2\text{S}_4$ (%): C, 56.38; H, 4.74; N, 3.28; found (%): C, 56.16; H, 4.73; N, 3.26.

3.5 | Preparation of Bis(*N*-furfuryl-*N*-methylferrocenyldithiocarbamato-*S,S'*)copper(II) (4)

A method similar to that described for the synthesis of **1** was adopted; however, *N*-furfuryl-*N*-methylferrocenylamine was used instead of *N*-(pyrrol-2-ylmethyl)-*N*-butylamine (Scheme 1). Synthesis and characterization of this complex have been reported earlier.^[13] To study its utility for the preparation of bimetallic sulfide nanoparticles, complex **4** was prepared using a slightly modified procedure. Colour: brown; yield: 78%; m.p. 170–172°C. IR (KBr, ν , cm^{-1}): 1487 ($\nu_{\text{C-N}}$), 1017 ($\nu_{\text{C-S}}$). UV-visible (CHCl_3 , λ , nm): 632, 437, 275, 228: Anal. Calcd for $\text{C}_{34}\text{H}_{36}\text{CuFe}_2\text{N}_2\text{O}_2\text{S}_4$ (%): C, 50.79; H, 4.01; N, 3.48; found (%): C, 50.62; H, 4.01; N, 3.45.

3.6 | Preparation of Copper and Copper-Iron Sulfide

An amount of 0.5 g of **2** was mixed with 15 ml of triethylenetetraamine in a round-bottom flask and then the contents of the flask were refluxed for 15 min. The black precipitate obtained was filtered off and washed with methanol.

A similar procedure was adopted for the preparation of copper-iron sulfide-**1** and copper-iron sulfide-**2** from complexes **3** and **4**.

4 | RESULTS AND DISCUSSION

4.1 | IR Spectral Studies

IR spectra of **1–4** are shown in Figures S1–S4 and the theoretical IR spectrum of **3** is displayed in Figure S5. The $\nu_{\text{C-S}}$ band in the range 950–1050 cm^{-1} is used to determine the mode of coordination of the dithiocarbamate ligand to the metal centre.^[27,28] The splitting of the $\nu_{\text{C-S}}$ band is characteristic of a monodentate dithiocarbamate ligand whereas the appearance of a single band in

this region is characteristic of bidentate chelation of dithiocarbamate ligands. The IR spectra of complexes **1–4** exhibit a distinct vibrational band at around 1020 cm^{-1} which is associated with the bidentate $\nu_{\text{C-S}}$ vibration of the dithiocarbamate ligands. The spectral band observed in the region 1450–1550 cm^{-1} is associated with $\nu_{\text{C-N}}$ vibrational mode. The position of this band in IR spectra in general is found between values for single (1250–1350 cm^{-1}) and double (1640–1690 cm^{-1}) bonds.^[29,30] For complexes **1–4**, the $\nu_{\text{C-N}}$ (thioureide) band appeared in the range 1487–1494 cm^{-1} , indicating the partial double bond character of C–N bond.^[31] While the calculated values of $\nu_{\text{C-S}}$ and $\nu_{\text{C-N}}$ vibrations are observed at 1488 and 1025 cm^{-1} for **3**. Additionally, the band observed at around 3380 cm^{-1} for complexes **1** and **2** is indicative of the free NH function in the pyrrole moiety.

4.2 | Electronic Spectral Studies

Electronic spectra of **1–4** are shown in Figures S6–S9. The electronic absorption spectra of the complexes are characterized by three absorption bands associated with the dithiocarbamate fragment. Two peaks observed in the range 225–275 nm are assigned to the $\pi \rightarrow \pi^*$ intraligand transitions of dithiocarbamate.^[32] The broad absorption bands of medium intensity with λ_{max} at around 435 nm in the spectra are associated with charge transfer transitions of the type ligand \rightarrow metal and metal \rightarrow ligand between Cu(II) ion and dithiocarbamate ligand.^[33,34] The weak and broad band with appearance of a shoulder in the region around 630–640 nm belongs to d–d transitions of Cu(II) (${}^2\text{B}_{1g} \rightarrow {}^2\text{E}_g$) in a square planar geometry.^[35]

4.3 | Single-Crystal X-ray Structural Analysis

Generally Cu(II) dithiocarbamate complexes display three types of structural motifs: they are (i) square planar monomeric,^[36,37] (ii) five-coordinate dimeric^[36,38] and (iii) infinite polymeric chain.^[39] Complex **3** was obtained as a monomeric species. XRD studies of **3** show that each copper atom is surrounded by four sulfur atoms from two chelating *N*-methylferrocenyl-*N*-(2-phenylethyl)dithiocarbamate ligands with isobidentate coordination mode (Figure 1). The Cu–S1, Cu–S2, Cu–S3 and Cu–S4 distances are approximately symmetric with values of 2.305, 2.298, 2.302 and 2.293 Å, respectively. The copper centre of **3** has a distorted square planar four-coordinate environment.^[14,40–42] The distortion is due to small bite angles of the chelating dithiocarbamates (S1–Cu–S2 = 77.56(2)° and S3–Cu–S4 = 77.75(2)°) which results in secondary deviations of the other angles from ideal square planar angles. The delocalization of π -

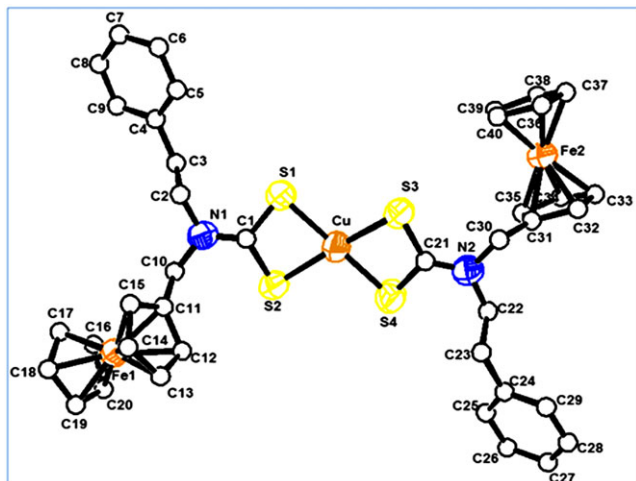


FIGURE 1 Molecular structure of complex 3

electron density over the S_2CN moiety is obvious from the shortening of the C—S (mean: 1.724 Å) and C—N (1.315 and 1.316 Å) bond lengths considering the typical C—N and C—S single bonds.^[2,14,40–42]

In complex 3, molecules pack through C14—H14 $\cdots\pi$ (2.766 Å) interaction between the monomers making up the polymeric chain (Figure 2; Table 3). There is also

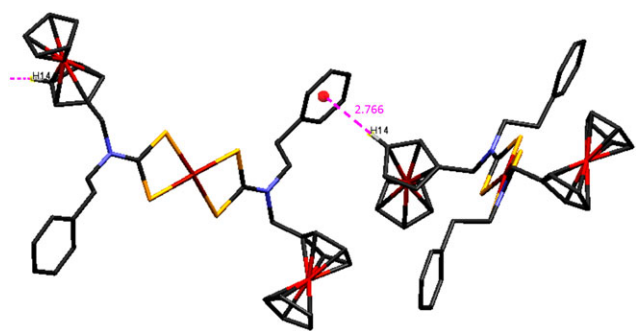


FIGURE 2 Intermolecular C—H $\cdots\pi$ interaction in 3

TABLE 3 Geometric details of hydrogen bonding (Å, °) in 3

Interactions	D—H (Å)	H \cdots A (Å)	D \cdots A (Å)	D—H \cdots A (°)
C2—H2B \cdots S1 ^a	0.97	2.630	3.021 (2)	104.41
C10—H10A \cdots S2 ^a	0.97	2.703	3.053 (2)	101.81
C30—H30B \cdots S3 ^a	0.97	2.560	3.083 (2)	113.85
C22—H22B \cdots S4 ^a	0.97	2.665	3.019 (2)	102.01
C3—H3A \cdots S4 ^b	0.97	2.795	3.753 (2)	169.06
C7—H7 \cdots S2 ^b	0.93	2.921	3.776 (3)	153.52
C14—H14 \cdots Cg(C24-C29) ^c	0.93	2.766	3.671	164.79
C39—H39 \cdots Cg(C16-C20) ^c	0.93	3.025	3.912	159.89

^aIntramolecular C—H \cdots S hydrogen bonding.

^bIntermolecular C—H \cdots S interactions.

^cIntermolecular C—H $\cdots\pi$ interactions.

formation of two intermolecular C—H \cdots S (C3—H3A \cdots S4 = 2.795 Å and C23—H23A \cdots S1 = 2.835 Å) bonds giving rise to a one-dimensional self-arrangement (Figure S10). A C39—H39 $\cdots\pi$ interaction occurs between H39 and a centroid of a cyclopentadienyl ring (C16–20). The parameters associated with this interaction are a H39–ring centroid distance of 3.025 Å and angle of 159.89° at H (Figure S11). The H7 atom forms an intermolecular C7—H7 \cdots S2 interaction with S2 which results in a polymeric chain structure (Figure S12). The ferrocene groups are linked as layers. The distances between two adjacent iron atoms are in the range 6.297–6.655 Å. In this layer, each ferrocene group is surrounded by four other ferrocene groups which are perpendicular to the central ferrocene group. The cyclopentadienyl planes in each ferrocene moiety are nearly parallel and the conformations nearly eclipsed. In this layer, the distance between H15 and H39 is 2.478 Å, a distance which shows the formation of rare closed-shell hydrogen–hydrogen interactions in 3 shorter than the sum of van der Waals radii for the hydrogen atoms^[43] (Figure 3). In complex 3, four intramolecular C—H \cdots S interactions occur between the hydrogen atoms of CH₂ and sulfur atoms (Figure S13).

5 | DFT STUDIES

5.1 | Molecular Geometry and Structural Properties

Figure S14 exhibits the optimized structure of complex 3 obtained from the B3LYP/LanL2DZ method. The selected optimized geometrical parameters of 3 from DFT method calculations and the XRD values are listed in Table 2. For 3, each copper atom is surrounded by four sulfur atoms from two chelating *N*-methylferrocenyl-*N*-(2-phenylethyl)dithiocarbamate ligands with bidentate coordination mode. The Cu—S1, Cu—S2, Cu—S3 and Cu—S4

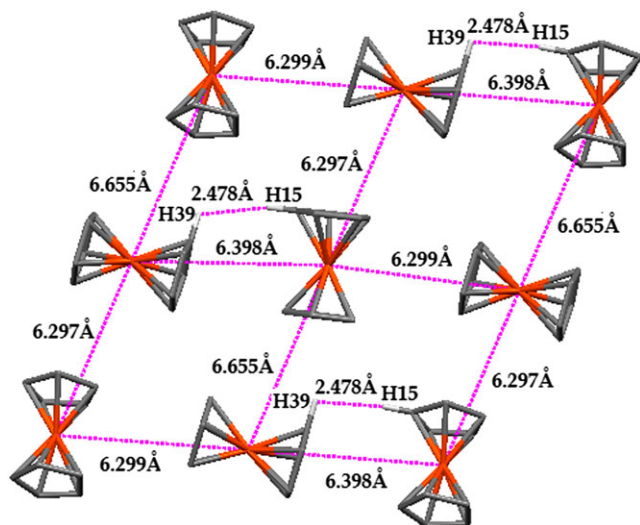


FIGURE 3 Layer formed via Fe...Fe interactions and H...H interactions in **3**

distances are approximately symmetric with values of 2.431, 2.492, 2.430 and 2.432 Å, respectively. A comparison of bond parameters (Table 2) of experimental and calculated values reveals that the differences between experimental and calculated bond lengths are in the range 0.03–0.07 Å except Cu—S bond distances (0.13–0.19 Å). Similarly the bond angles are almost equal for both methods (0.35–1.5°) except S2—Cu—S3 (9.87°) and S4—Cu—S1 (3.03°). These differences between bond parameters arise due to the calculated geometric parameters using the DFT method considering the gas phase only and that the molecule is free of interactions.

5.2 | Frontier Molecular Orbital Analysis

The HOMO and LUMO are the most important orbitals in a molecule. HOMO is mainly located over four sulfur atoms and the LUMO of π nature is delocalized over both the MS₂CN rings (Figure 4). The hardness (η), chemical potential (μ) and electronegativity (χ) are calculated using HOMO and LUMO energies. For complex **3**, $\eta = 2.2611$ eV, $\mu = -3.4583$ eV and $\chi = 3.4583$ eV.^[44] It is seen that the chemical potential of **3** is negative. This indicates that the complex is stable. The hardness signifies the resistance towards the deformation of electron clouds of chemical systems under small perturbations encountered during chemical processes.

5.3 | Molecular Electrostatic Potential

The various values of the electrostatic potential at the molecular electrostatic potential surfaces are represented by different colours. Potential increases in the order red (negative potential) < orange < yellow (zero potential)

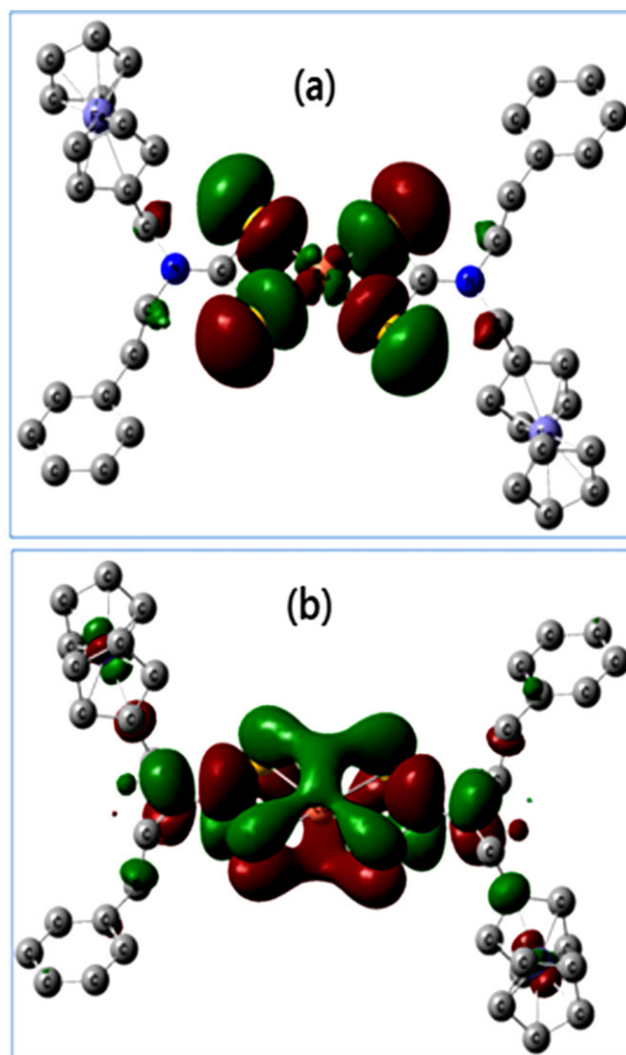


FIGURE 4 Graphical images of (a) HOMO and (b) LUMO of complex **3**

< green < blue (positive potential). The blue colour indicates the strongest attraction of electrons and red indicates the strongest repulsion of electrons.^[45,46] The molecular electrostatic potential map of **3** (Figure S15) shows that regions having negative potential are over the four S atoms and the regions having the positive potential are over the two N atoms. This supports the presence of canonical structure R₁R₂N⁺—CS₂²⁻.

6 | ANION BINDING STUDIES

The recognition ability of **1** towards halide ions in the form of their corresponding tetrabutylammonium salts was investigated using cyclic voltammetry in CH₃CN solution containing 0.01 M tetrabutylammonium fluoroborate as a supporting electrolyte. Complex **1** shows a one-electron quasi-reversible Cu(II) to Cu(I) reductive response (Figure 5). Similar observations for copper(II)

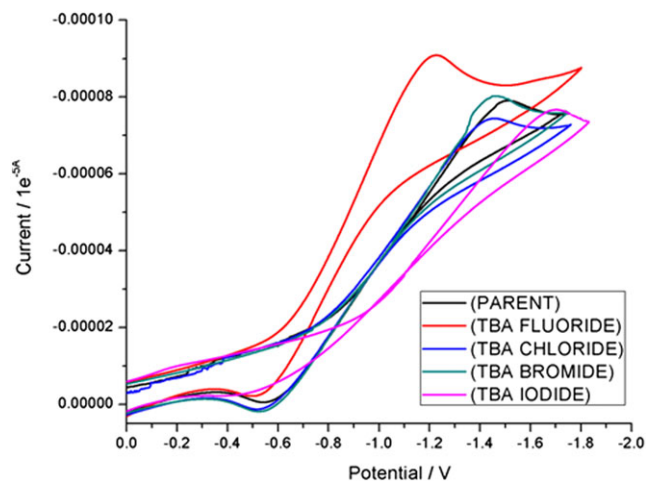


FIGURE 5 Changes in cyclic voltammogram of complex **1** on the addition of anions (TBA, tetrabutylammonium)

dithiocarbamates were reported by Gupta *et al.*^[35] Complex **1** exhibits a marked electrochemical change to F^- ($\Delta E_{1/2} = 0.2689$ V) followed by I^- ($\Delta E_{1/2} = 0.2011$ V) (Table 4). In contrast, addition of the other anions to a CH_3CN solution of complex **1** does not induce any significant change in the signals of cyclic voltammogram of complex **1**.

7 | CHARACTERIZATION OF COPPER SULFIDE AND COPPER-IRON SULFIDE NANOPARTICLES

Copper sulfide and copper-iron sulfide nanoparticles obtained from complexes **2**, **3** and **4** are represented as copper sulfide, copper-iron sulfide-**1** and copper-iron sulfide-**2**, respectively. The XRD patterns of copper sulfide and copper-iron sulfides are shown in Figure S16. The diffraction pattern of the dominant phase in copper sulfide is cubic Cu_9S_5 with major diffraction peaks of (0015), (1010), (0114), (110), (0027), (1112) and (2017) planes (JCPDS card no. 47-1748). The diffraction patterns of copper-iron sulfide-**1** are indexed to the cubic phase of Cu_5FeS_4 with characteristic (111), (200), (220), (331) and

TABLE 4 Electrochemical anion recognition data of complex **1**

Compound ^a	E_{pc} (V)	$\Delta E_{1/2}$ (V) ^b
Complex	-1.5024	—
TBA fluoride	-1.2331	0.2693
TBA chloride	-1.4485	0.0539
TBA bromide	-1.4635	0.0389
TBA iodide	-1.7035	0.2011

^aTBA, tetrabutylammonium.

^bShift of $Cu(II)/Cu(I)$ reduction potential produced by anions.

(222) planes (JCPDS card no, 73-1667). In the case of copper-iron sulfide-**2**, the diffraction peaks at $2\theta = 29.45^\circ$, 48.67° and 58.0° are assigned to the (111), (220) and (311) planes of cubic structure (JCPDS card no. 81-1378). The XRD patterns of copper sulfide and copper-iron sulfide-**1** are of poor quality being indicative of low crystallinity and the presence of other phases.

The morphologies of the as-prepared metal sulfide nanoparticles were investigated by TEM analysis. TEM images of copper sulfide and copper-iron sulfides are shown in Figure 6. The TEM images of copper sulfide particles obtained from complex **2** show that they are spherical with diameters in the range 10–18 nm (Figure 6a,b). The TEM image of copper-iron sulfide-**1** reveals that the shapes of the particles are spherical (diameters of 11–20 nm; Figure 6c). The shape of the copper-iron sulfide-**2** nanoparticles is oval morphology (Figure 6d,e).

The elemental composition of copper sulfide and copper-iron sulfide nanoparticles was investigated. EDS spectra of products obtained from complexes **2**, **3** and **4** are shown in Figure S17. The EDS trace of the product obtained from solvothermal decomposition of complex **2** reveals the formation of copper sulfide. The Cu:S atomic ratio (9:5.6) shows that there are some vacancies of Cu^{2+} ions or some sulfur dangling bonds are present in the sample. EDS analysis of copper-iron sulfide-**1** and -**2** indicates the presence of two metals (Cu and Fe) and sulfur. The Cu:Fe:S ratio of copper-iron sulfide-**1** and -**2** are 3.5:1.0:3.7 and 1.0:2.0:2.7, respectively.

The expected Cu:S and Cu:Fe:S ratios for copper sulfide (Cu_9S_5) and copper-iron sulfide -**1** (Cu_5FeS_4) from powder XRD studies are 9:5 and 5:1:4, respectively. But the ratios observed from EDS are different. This supports the presence of various phases. In the case of copper-iron sulfide-**2** ($CuFe_2S_3$) the ratios of Cu:Fe:S determined from powder XRD (1:2:3) and EDS (1:2:2.7) are almost the same.

Figure S18 illustrates the UV-visible absorption spectra of copper sulfide and copper-iron sulfide nanoparticles dispersed in distilled ethanol at room temperature. A broad band appears at 272 nm (4.56 eV) for copper sulfide whereas a band at 270 nm (4.59 eV) and a weak band at 260 nm (4.77 eV) are observed for copper-iron sulfide-**1** and -**2**, respectively. Compared with bulk copper sulfide (1033 nm, 1.2 eV),^[47] the absorption maxima of copper sulfide and copper-iron sulfide nanoparticles exhibit a large blue shift, which is attributed to the quantum confinement of charge carriers in the nanoparticles.

Figures S19 and S20 show the photoluminescence spectra recorded at room temperature for copper sulfide and copper-iron sulfide-**2** nanoparticles. The emission

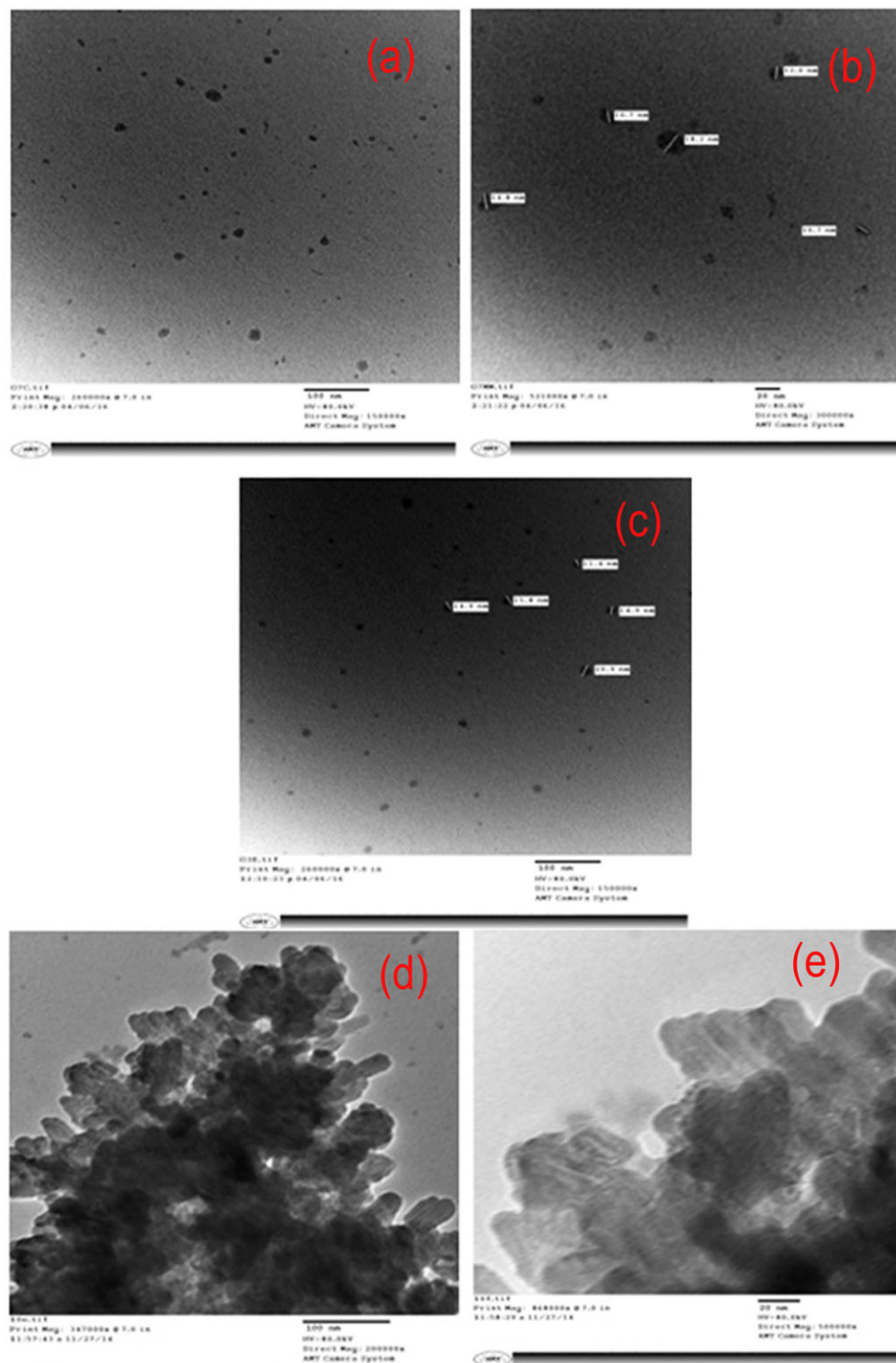


FIGURE 6 TEM images of copper sulfide, scale bars (a) 100 nm and (b) 20 nm; copper-iron sulfide-1 (c); and copper-iron sulfide-2, scale bars (d) 100 nm and (e) 20 nm

spectra of both types of nanoparticles exhibit a peak at around 400 nm corresponding to the band-edge emission. Along with this emission another red-shifted intense peak is observed at 432 nm in the spectrum of copper-iron sulfide-2. The red-shifted emission results from trap-related electron-hole recombination.

IR spectra of copper sulfide and copper-iron sulfide nanoparticles (Figures S21–S23) exhibit three bands in the region $2850\text{--}2964\text{ cm}^{-1}$ due to aliphatic $\nu_{\text{C-H}}$. The bands in the region $3415\text{--}3485\text{ cm}^{-1}$ are assigned to N–H stretching vibrations. These data indicate the presence of triethylenetetraamine capping agent in

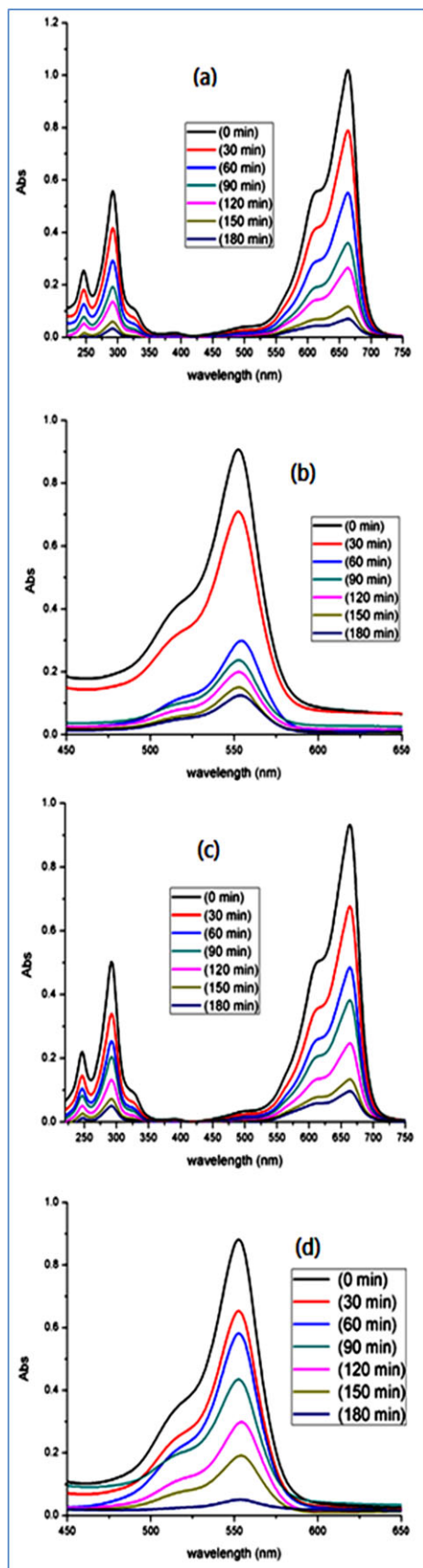


FIGURE 7 Absorption spectral changes of methylene blue and rhodamine-B using (a, b) copper sulfide and (c, d) copper-iron sulfide-1 under UV light

copper sulfide and copper-iron sulfide-1 and -2. The lack of aromatic C—H and N—CS₂ stretching vibrations indicates the absence of dithiocarbamate ligands in the as-synthesized copper-iron sulfide nanoparticles.

7.1 | Photocatalytic Activity of Copper Sulfide and Copper-Iron Sulfide

The photocatalytic activity performances of as-prepared copper sulfide and copper-iron sulfide-1 were evaluated by photocatalytic degradation of methylene blue and rhodamine-B aqueous solutions. The degradation of methylene blue and rhodamine-B was carried out using UV irradiation as followed by spectrophotometric monitoring. Figure 7 shows the temporal evolution of the absorption spectra during the photocatalytic degradation of methylene blue and rhodamine-B in the presence of copper sulfide and copper-iron sulfide-1. As the irradiation time increased the absorption peaks decreased. Figure 8 shows the photodegradation efficiency of methylene blue and rhodamine-B as a function of irradiation time. C is the absorption of methylene blue and rhodamine-B at 662 and 554 nm, respectively, at time t and C_0 is the absorption of methylene blue and rhodamine-B before irradiation.

The experiments showed the good photocatalytic activity of copper sulfide and copper-iron sulfide-1 for the degradation of methylene blue and rhodamine-B under UV irradiation. It was observed that copper sulfide degraded 89% of methylene blue in 180 min while copper-iron sulfide-1 degraded 93% of methylene blue in 180 min under UV light. It was also observed that copper sulfide and copper-iron sulfide degraded 82 and 86% of

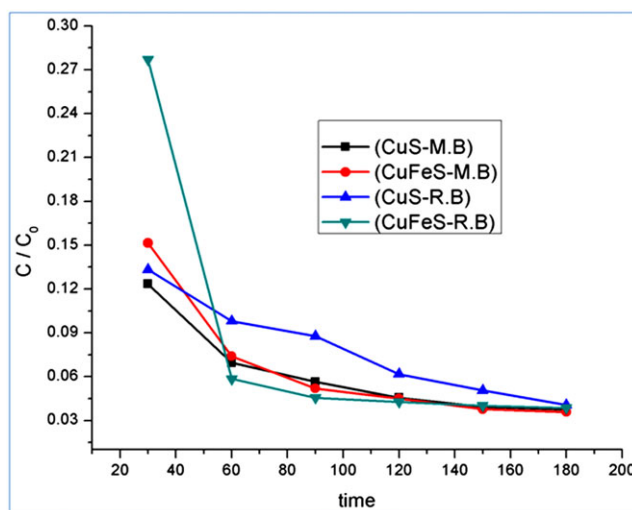


FIGURE 8 Photocatalytic degradation of methylene blue (M.B.) and rhodamine-B (R.B.) using copper sulfide and copper-iron sulfide-1

rhodamine-B, respectively, under UV light irradiation in 180 min. The degradation efficiency of copper-iron sulfide is greater than that of copper sulfide for the investigated dyes. The presence of iron in copper-iron sulfide-**1** can also enhance the photocatalytic degradation activity due to smaller crystal size, higher efficiency for electron-hole regeneration and charge trapping.

8 | CONCLUSIONS

Complexes **1–4** containing pyrrole and ferrocene moieties were prepared and characterized. The copper centre in **3** has distorted square planar four-coordinate environments. The chemical potential of **3** calculated using DFT is negative (−3.4583 eV). This indicates that the complex is stable. Anion binding studies show that complex **1** prefers to bind with F[−]. This study demonstrates that spherical copper sulfide and copper-iron sulfide nanoparticles and oval-shaped copper-iron sulfide nanoparticles can be prepared from the copper dithiocarbamate complexes. Copper-iron sulfide (bimetallic) nanoparticles revealed better photocatalytic activity for the photodegradation of methylene blue and rhodamine-B under UV light compared to copper sulfide (monometallic). This study indicates that the new copper(II) dithiocarbamate complexes containing various N-bound organic moieties are useful for sensing anions and for preparing effective photocatalysts (copper sulfide and copper-iron sulfide nanoparticles with various shapes).

ACKNOWLEDGEMENTS

S.T. is grateful to the University Grants Commission (UGC), India (no. 42-341/2013 (SR)) for providing funding for this research study. We are grateful to SAIF, Panjab University, Chandigarh, India, for recording TEM images.

ORCID

Subbiah Thirumaran  <http://orcid.org/0000-0002-5771-5328>

REFERENCES

- [1] P. J, *Prog. Inorg. Chem.* **2005**, 53, 1.
- [2] G. Hogarth, *Prog. Inorg. Chem.* **2005**, 53, 71.
- [3] F. H. Allen, *Acta Crystallogr B* **2002**, 58, 71.
- [4] F. Shaheen, A. Badshah, M. Gielen, C. Gieck, M. Jamil, D. de Vos, *J. Organometal. Chem.* **2008**, 693, 1117.
- [5] V. Alverdi, L. Giovagnini, C. Marzano, R. Seraglia, F. Bettio, S. Sitran, R. Graziani, D. Fregona, *J. Inorg. Biochem.* **2004**, 98, 1117.
- [6] R. Singh, N. K. Kaushik, *Spectrochim. Acta Mol. Biomol. Spectrosc.* **2008**, 71, 669.
- [7] A. M. Bond, R. L. Martin, *Coord. Chem. Rev.* **1984**, 54, 23.
- [8] A. R. Hendrickson, R. L. Martin, N. M. Rohde, *Inorg. Chem.* **1976**, 15, 2115.
- [9] J. Cookson, P. D. Beer, *Dalton Trans.* **2007**, 1459.
- [10] G. Gurumoorthy, S. Thirumaran, *Phosphorus, Sulfur Silicon Relat. Elem.* **2017**, 192, 330.
- [11] P. Li, K.-Y. Qui, *J. Polym. Sci., Polym. Chem.* **2002**, 40, 2093.
- [12] P. Li, K.-Y. Qui, *Macromolecules* **2002**, 35, 8906.
- [13] V. Singh, R. Chauhan, A. N. Gupta, V. Kumar, M. G. B. Drew, L. Bahadur, N. Singh, *Dalton Trans.* **2014**, 43, 4752.
- [14] P. D. Beer, N. Berry, M. G. B. Drew, O. D. Fox, M. E. Padilla-Tosta, S. Patell, *Chem. Commun.* **2001**, 199.
- [15] R. Nomura, K. Miyakawa, T. Toyosaki, H. Matsuda, *Chem. Vap. Deposition* **1996**, 2, 174.
- [16] M. Kemmler, M. Lazell, P. O'Brien, D. J. Otway, J.-H. Park, J. R. Walsh, *J. Mater. Sci. Mater. Electron* **2002**, 13, 531.
- [17] P. O'Brien, J. R. Walsh, I. M. Watson, L. Hart, S. R. P. Silva, *J. Cryst. Growth* **1996**, 167, 133.
- [18] M. R. Lazell, P. O'Brien, D. J. Otway, J.-H. Park, *Chem. Mater.* **1999**, 11, 3430.
- [19] A. L. Abdelhady, K. Ramasamy, M. A. Malik, P. O'Brien, S. J. Haigh, J. Raftery, *J. Mater. Chem* **2011**, 21, 17888.
- [20] T. Okubo, R. Kawajiri, T. Mitani, T. Shimoda, *J. Am. Chem. Soc.* **2005**, 127, 17598.
- [21] R. H. Bube, W. H. McCarroll, *J. Phys. Chem. Solids* **1959**, 10, 333.
- [22] D. V. Konarev, A. Y. Kovalevsky, D. V. Lopatin, A. V. Umrikhin, E. I. Yudanov, P. Coppens, R. N. Lyubovskaya, G. Saito, *Dalton Trans.* **2005**, 1821.
- [23] V. F. Plyusnin, A. V. Kolomeets, V. P. Grivin, S. V. Larionov, H. Lemmetyinen, *J. Phys. Chem. A* **2011**, 115, 1763.
- [24] G. M. Sheldrick, *Acta Crystallogr. C* **2015**, 71, 3.
- [25] M. J. Frisch, G. W. Trucks, H. B. Schlegel, G. E. Scuseria, M. A. Robb, J. R. Cheeseman, J. A. Montgomery, Jr., T. Vreven, K. N. Kudin, J. C. Burant, J. M. Millam, S. S. Iyengar, J. Tomasi, V. Barone, B. Mennucci, M. Cossi, G. Scalmani, N. Rega, G. A. Petersson, H. Nakatsuji, M. Hada, M. Ehara, K. Toyota, R. Fukuda, J. Hasegawa, M. Ishida, T. Nakajima, Y. Honda, O. Kitao, H. Nakai, M. Klene, X. Li, J. E. Knox, H. P. Hratchian, J. B. Cross, C. Adamo, J. Jaramillo, R. Gomperts, R. E. Stratmann, O. Yazyev, A. J. Austin, R. Cammi, C. Pomelli, J. W. Ochterski, P. Y. Ayala, K. Morokuma, G. A. Voth, P. Salvador, J. J. Dannenberg, V. G. Zakrzewski, S. Dapprich, A. D. Daniels, M. C. Strain, O. Farkas, D. K. Malick, A. D. Rabuck, K. Raghavachari, J. B. Foresman, J. V. Ortiz, Q. Cui, A. G. Baboul, S. Clifford, J. Cioslowski, B. B. Stefanov, G. Liu, A. Liashenko, P. Piskorz, I. Komaromi, R. L. Martin, D. J. Fox, T. Keith, M. A. Al-Laham, C. Y. Peng, A. Nanayakkara, M. Challacombe, P. M. W. Gill, B. Johnson, W. Chen, M. W. Wong, C. Gonzalez, J. A. Pople, *Gaussian 03, Revision B.03*, Gaussian Inc., Pittsburgh, PA **2003**.

- [26] E. Sathiyaraj, G. Gurumoorthy, S. Thirumaran, *New J. Chem.* **2015**, 39, 5336.
- [27] F. Bonati, R. Ugo, *J. Organometal. Chem.* **1967**, 10, 257.
- [28] L. Ronconi, L. Giovagnini, C. Marzano, F. Bettio, R. Graziani, G. Pilloni, D. Fregona, *Inorg. Chem.* **2005**, 44, 1867.
- [29] J. O. Hill, R. J. Magee, *Rev. Inorg. Chem.* **1981**, 3, 141.
- [30] A. W. Herlinger, S. L. Wenholt, T. V. Long, *J. Am. Chem. Soc.* **1970**, 92, 6474.
- [31] J. Criado, I. Fernandez, B. Macias, J. M. Salas, M. Medarde, *Inorg. Chim. Acta* **1990**, 174, 67.
- [32] N. Manav, A. K. Mishra, N. K. Kaushik, *Spectrochim. Acta A* **2006**, 65, 32.
- [33] C. K. Jorgensen, *J. Inorg. Nucl. Chem.* **1962**, 24, 1571.
- [34] D. Coucouvanis, *Prog. Inorg. Chem.* **1980**, 26, 302.
- [35] A. N. Gupta, V. Singh, V. Kumar, A. Rajput, L. Singh, M. G. B. Drew, N. Singh, *Inorg. Chim. Acta* **2013**, 408, 145.
- [36] G. M. de Lima, D. C. Menezes, C. A. Cavacanti, J. A. F. dos Santos, I. P. Ferreira, E. B. Paniago, J. L. Wardell, S. M. S. V. Wardell, K. Krambrock, I. C. Mendes, *J. Mol. Struct.* **2011**, 988, 1.
- [37] I. P. Ferreira, G. M. de Lima, E. B. Paniago, J. A. Takahashi, K. Krambrock, C. B. Pinheiro, J. L. Wardell, L. C. Visentin, *J. Mol. Struct.* **2013**, 1048, 357.
- [38] F. F. Jain, Z. X. Wang, Z. P. Bai, X. Z. You, H. K. Fun, K. Chinnakali, I. A. Razak, *Polyhedron* **1999**, 18, 3401.
- [39] F. W. B. Einstein, J. S. Field, *Acta crystallogr. B*, **2929**, 1974, 30.
- [40] S. C. Ngo, K. K. Banger, M. J. DelaRosa, P. J. Toscano, J. T. Welch, *Polyhedron* **2003**, 22, 1575.
- [41] A. Meleros, A. Cachapa, R. Hernantoz-Molina, M. T. Armas, P. Gili, M. Sokolov, J. Gonzalez-Plates, F. Brito, *Inorg. Chem. Commun.* **2003**, 6, 498.
- [42] W. E. Hatfield, P. Singh, F. Nepveu, *Inorg. Chem.* **1990**, 29, 4214.
- [43] C. F. Matta, J. Hernandez-Trujillo, T.-H. Tang, R. F. W. Bader, *Chem. – Eur. J.* **2003**, 9, 1940.
- [44] A. Bendjeddou, T. Abbaz, A. Gouasmia, D. Villemin, *Am. J. Appl. Chem.* **2016**, 4, 104.
- [45] J. Luque, J. M. Lopez, M. Orozco, *Theor. Chem. Acc.* **2000**, 103, 343.
- [46] E. Scrocco, J. Tomas, *Adv. Quantum Chem.* **1978**, 11, 115.
- [47] Q. W. Tian, M. H. Tang, Y. G. Sun, R. J. Zou, Z. G. Chen, M. F. Zhu, S. P. Yang, J. L. Wang, J. H. Wang, J. Q. Hu, *Adv. Mater.* **2011**, 23, 3542.

SUPPORTING INFORMATION

Additional Supporting Information may be found online in the supporting information tab for this article.

How to cite this article: Gurumoorthy G, Thirumaran S, Ciattini S. Synthesis and characterization of copper(II) dithiocarbamate complexes involving pyrrole and ferrocenyl moieties and their utility for sensing anions and preparation of copper sulfide and copper-iron sulfide nanoparticles. *Appl Organometal Chem.* 2018;e4363. <https://doi.org/10.1002/aoc.4363>